Journal of Organometallic Chemistry 694 (2009) 3091–3101

Contents lists available at ScienceDirect

Journal of Organometallic Chemistry

journal homepage: www.elsevier.com/locate/jorganchem

Synthesis, crystal structure, antioxidation and DNA binding properties of binuclear Ho(III) complexes of Schiff-base ligands derived from 8-hydroxyquinoline-2-carboxyaldehyde and four aroylhydrazines

Yong-chun Liu [a,b], Zheng-yin Yang [a,*]

[a] College of Chemistry and Chemical Engineering, State Key Laboratory of Applied Organic Chemistry, Lanzhou University, Lanzhou 730000, PR China
[b] College of Chemistry and Chemical Engineering, Longdong University, Qingyang, Gansu 745000, PR China

ARTICLE INFO

Article history:
Received 5 February 2009
Received in revised form 18 May 2009
Accepted 21 May 2009
Available online 27 May 2009

Keywords:
Rare earth
Schiff-base
8-Hydroxyquinoline-2-carboxyaldehyde
X-ray crystallography
Calf thymus DNA binding properties
Antioxidation

ABSTRACT

X-ray crystal and other structural analyses indicate that Ho(III) and every newly synthesized ligand can form a binuclear Ho(III) complex with a 1:1 metal-to-ligand stoichiometry by nine-coordination at the Ho(III) center. Every ligand acts as a dibasic tetradentate ligand, binding to Ho(III) through the phenolate oxygen atom, nitrogen atom of quinolinato unit and the C=N group, $^{-}$O–C=N– group (enolized and deprotonated from O=C–NH– group) of the aroylhydrazine side chain. One DMF molecule is binding orthogonally to the ligand-plane from one side to the metal ion, while another DMF and nitrate (bidentate) are binding from the other. Dimerization of this monomeric unit occurs through the phenolate oxygen atoms leading to a central planar four-membered $(HoO)_2$ ring. Investigations of DNA binding properties show that all the ligands and Ho(III) complexes can bind to Calf thymus DNA through intercalations with the binding constants at the order of magnitude 10^5–10^6 M^{-1}, but Ho(III) complexes present stronger affinities to DNA than ligands. All the ligands and Ho(III) complexes may be used as potential anticancer drugs. Investigations of antioxidation properties show that all the ligands and Ho(III) complexes have strong scavenging effects for hydroxyl radicals and superoxide radicals but Ho(III) complexes show stronger scavenging effects for hydroxyl radicals than ligands.

1. Introduction

It is demonstrated that DNA is one of the primary intracellular targets of anti-cancer drugs due to the interaction of small molecules with DNA, which causes DNA damage in cancer cells, inhibit the division of cancer cells and result in cell death [1,2]. This is the basis of designing new and more efficient antitumor drugs and their effectiveness depends on the mode and affinity of the binding [3–5]. A number of metal chelates, as agents for mediation of strand scission of duplex DNA and as chemotherapeutic agents, have been used as probes of DNA structure in solution [6–8]. Apart from the magnetic and photophysical properties, the bioactivities of lanthanides such as antimicrobial, antitumor, antivirus, anticoagulant action, enhancing NK and Macrophage cell activities and prevention from arteriosclerosis, have been explored in recent decades [9–12]. In addition, Schiff-bases are able to inhibit the growth of several animal tumors, and some metal chelates have shown good antitumor activities against animal tumors [13,14]. So, well designed organic ligands enable a fine tuning of special properties of the metal ions. The chemistry of quinoline and its derivatives has also attracted special interest due to their therapeutic properties. Quinoline sulphonamides have been used in the treatment of cancer, tuberculosis, diabetes, malaria, and convulsion [15,16]. Albrecht and coworkers reported that the crystal structures of $[YL(NO_3)(DMF)_2]_2Cl_2{\cdot}2(DMF)$ and $[LaL(NO_3)(MeOH)_2]_2(NO_3)_2$ with nine-coordination have central planar four-membered $(LaO)_2$ and $(YbO)_2$ rings, respectively, where ligand L–H is 2-[(8-hydroxyquinolinyl)methylene]hydrazinecarboxamide and acts as a tetradentate ligand binding to yttrium(III) and lanthanum(III) [10]. Such structures may have strong affinities of binding to DNA through intercalation. In this paper, four Schiff-base ligands, which were structurally similar to the ligand L–H, were prepared from 8-hydroxyquinoline-2-carboxyaldehyde with four aroylhydrazines to form their Ho(III) complexes and to investigate the DNA binding properties.

On the other hand, an excess of activated oxygen species in the forms of superoxide anion ($O_2^{\cdot -}$) and hydroxyl radical ($OH^{\cdot}$), generated by normal metabolic processes, may cause various diseases such as carcinogenesis, drug-associated toxicity, inflammation, atherogenesis, and aging in aerobic organisms [17–19]. Although the naturally occurring antioxidants can scavenge free radicals in the body, they have been limited by their low effectiveness even though they are considered to be active in eliminating reactive

* Corresponding author. Tel.: +86 931 8913515; fax: +86 931 8912582.
E-mail address: yangzy@lzu.edu.cn (Z.-y. Yang).

0022-328X/$ - see front matter © 2009 Elsevier B.V. All rights reserved.
doi:10.1016/j.jorganchem.2009.05.031

oxygen and controlling toxic effects. The potential value of antioxidants has prompted investigators to search for the cooperative effects of metal complexes and natural compounds for improving antioxidant activity and cytotoxicity [20]. It has been recently demonstrated that some DNA binders are effective inhibitors of the formation of a DNA/TBP complex or topoisomerases [21–23]. Adding a reactive entity endowed with oxidative properties should improve the efficiency of inhibitors. The antioxidation properties of the ligands and Ho(III) complexes were investigated in this paper. Furthermore, the substituent effects of these compounds on antioxidation and DNA binding properties were investigated further.

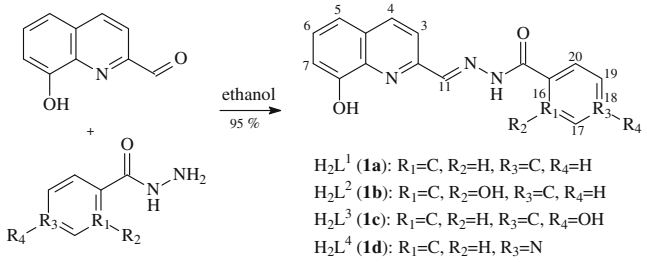

Scheme 1. The synthetic routes for ligands (**1a–d**).

Table 1
Crystal data and structure refinement of metal complexes.

Complex	$[HoL^1(NO_3)(DMF)_2]_2$	$3[HoL^4(NO_3)(DMF)_2]_2{\cdot}7(DMF)$
CCDC deposition number	735980	735981
Chemical formula	$C_{46}H_{50}N_{12}O_{14}Ho_2$	$C_{153}H_{193}N_{49}O_{49}Ho_6$
Formula weight	1324.84	4492.14
Crystal colour	Orange	Orange
Crystal size (mm)	0.32 × 0.29 × 0.23	0.25 × 0.24 × 0.21
T (K)	296(2)	296(2)
Wavelength (Å)	0.71073	0.71073
Radiation	Mo Kα	Mo Kα
Crystal system	Monoclinic	Rhombohedral
Space group	$P2_1/c$	$R-3$
Z	2	3
a (Å)	11.3770(7)	39.0005(18)
b (Å)	18.6475(11)	39.0005(18)
c (Å)	12.2552(7)	11.1457(7)
α (°)	90.00	90
β (°)	92.2710(10)	90
γ (°)	90.00	120
V (Å^3)	2597.9(3)	14681.8(13)
D_{calc} (g cm^{-3})	1.694	1.524
μ (mm^{-1})	3.099	2.481
F(0 0 0)	1312	6744
$\theta_{min/max}$ (°)	1.79–27.00	1.81–26.50
Index ranges	$-14 \leqslant h \leqslant 14$, $-23 \leqslant k \leqslant 22$, $-15 \leqslant l \leqslant 11$	$-48 \leqslant h \leqslant 41$, $-48 \leqslant k \leqslant 48$, $-13 \leqslant l \leqslant 13$
Reflections collected	14 732	27 740
Independent reflections [R_{int}]	5488 [0.0253]	6765 [0.0288]
Absorption correction	Semi-empirical from equivalents	Semi-empirical from equivalents
Maximum and minimum transmission	0.385 and 0.491	0.543 and 0.594
Refinement method	Full-matrix least-squares on F^2	Full-matrix least-squares on F^2
Data/restraints/parameters	5616/0/338	6765/0/411
Goodness-of-fit on F^2	1.048	1.055
Final R indices [$I > 2\sigma(I)$]	R_1 = 0.0221, wR_2 = 0.0479	R_1 = 0.0287, wR_2 = 0.0799
R indices (all data)	R_1 = 0.0341, wR_2 = 0.0532	R_1 = 0.0365, wR_2 = 0.0830
$\rho_{min/max}$ (e Å^{-3})	0.653 and −0.500	0.479 and −0.974

2. Results and discussion

2.1. Chemical syntheses of ligands and Ho(III) complexes

Four Schiff-base ligands, 8-hydroxyquinoline-2-carboxyaldehyde-(benzoyl)hydrazone (H_2L^1, **1a**), 8-hydroxyquinoline-2-carboxyaldehyde-(2′-hydroxybenzoyl)hydrazone (H_2L^2, **1b**), 8-hydroxyquinoline-2-carboxyaldehyde-(4′-hydroxybenzoyl)hydrazone (H_2L^3, **1c**) and 8-hydroxyquinoline-2-carboxyaldehyde-(isonicotinyl)hydrazone (H_2L^4, **1d**) were prepared from equimolar amounts of 8-hydroxyquinoline-2-carboxyaldehyde and benzoylhydrazine, 2-hydroxybenzoylhydrazine, 4-hydroxybenzoylhydrazine, and isonicotinylhydrazine, respectively. Their structures were determined by IR spectroscopy, ^{1}H NMR and ESI-MS. The synthetic routes for ligands are presented in Scheme 1. Then, the Ho(III) complexes (**2a–d**) were prepared from these ligands and equimolar amounts of $Ho(NO_3){\cdot}6H_2O$, respectively.

2.2. Crystal structure analyses of the Ho(III) complexes

The orange transparent, X-ray quality crystals of complex **2a** and **2d** were obtained by vapor diffusion of diethyl ether into DMF solution of the powdered complex at room temperature for 2 weeks, respectively. Crystal data and structure refinements for the X-ray structural analyses are presented in Table 1. Selected bond lengths and angles of the metal complexes are presented in Supplementary material Tables S1 and S2.

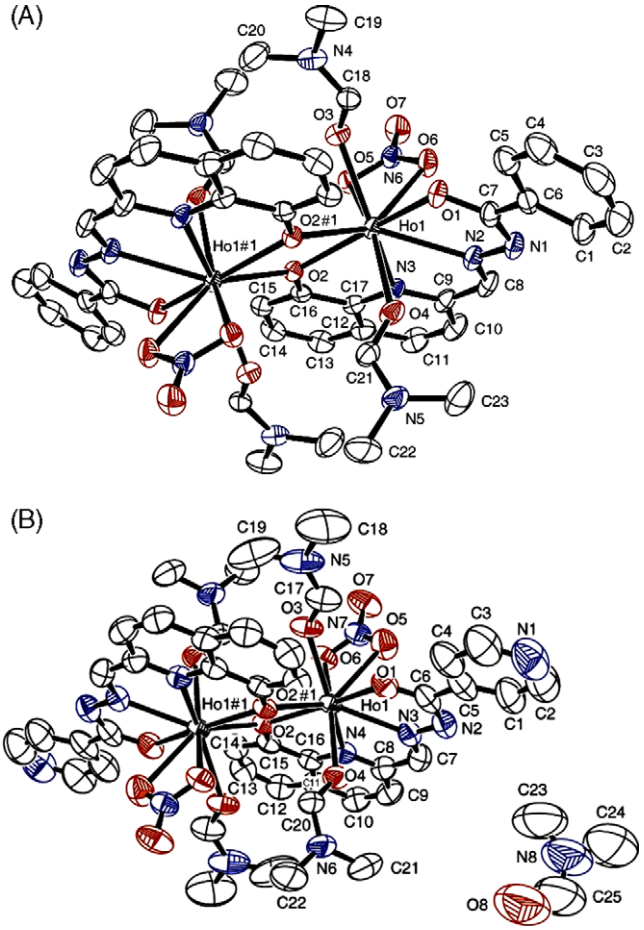

Fig. 1. Coordination spheres of ORTEP diagrams (30% probability ellipsoids) of $[HoL^1(NO_3)(DMF)_2]_2$ (A) and $3[HoL^4(NO_3)(DMF)_2]_2{\cdot}7(DMF)$ (B, unitary crystal structure) complexes.

*2.2.1. The crystal structure of complex **2a***

The coordination sphere of ORTEP diagram (30% probability ellipsoids) in Fig. 1A shows that the composition of complex **2a** is of $[HoL^1(NO_3)(DMF)_2]_2$. Ligand **1a** acts as a dibasic tetradentate ligand, binding to Ho(III) through the phenolate oxygen atom, nitrogen atom of quinolinato unit and the C=N group, $^-$O–C=N– group (enolized and deprotonated from O=C–NH–) of the benzoylhydrazine side chain. In addition, one DMF molecule is binding orthogonally to the ligand-plane from one side to the metal ion, while another DMF and nitrate (bidentate) are binding from the other. Dimerization of this monomeric unit occurs through the phenolate oxygen atoms leading to a central planar four-membered $(HoO)_2$ ring with a Ho···Ho separation of 3.990 Å. At the dimerization site, a "set off" of the two parallel "HoL^1-planes" by 1.615 Å takes place. This crystal structure of binucleae $[HoL^1(NO_3)(DMF)_2]_2$ complex with a 1:1 metal-to-ligand stoichiometry by nine-coordination is similar to that of $[YL(NO_3)(DMF)_2]_2Cl_2{\cdot}2(DMF)$ or $[LaL(NO_3)(MeOH)_2]_2(NO_3)_2$, where ligand L–H is 2-[(8-hydroxyquinolinyl)methylene]hydrazinecarboxamide and acts as a monad tetradentate ligand binding to yttrium(III) or lanthanum(III) through the phenolate oxygen atom, nitrogen atom of quinolinato unit and the C=N group, C=O group of the semicarbazone side chain [10]. However, there are two marked differences between them. One is that the "set off" of the two parallel "HoL^1-planes" by 1.615 Å takes place while both the "set off" of the two parallel "YL-planes" and "LaL-planes" by accurately 1.887 (CCDC 273601) and 1.388 Å (CCDC 273600) take place as shown in Table 2, respectively, though they were reported by approximately 2 Å. Another is that O=C–NH– group of the benzoylhydrazine side chain has enolized and deprotonated into $^-$O–C=N– group after the formation of $[HoL^1(NO_3)\ (DMF)_2]_2$ complex, where the C–O$^-$ band length is 1.287(3) Å and the N=C double band length is 1.316(4) Å (The normal band lengths of C=O, C–N, C–O and C=N are 1.19–1.23, 1.47–1.50, 1.30–1.39 and 1.34–1.38 Å, respectively [24]). Whereas carbonyl groups C=O of the semicarbazone side chain has not enolized in $[YL(NO_3)(DMF)_2]_2Cl_2{\cdot}2(DMF)$ or $[LaL(NO_3)(MeOH)_2]_2(NO_3)_2$ complex. The differences in the deprotonization and enolization may well be due to the fact that triethylamine was added into the reaction mixtures to deprotonate the phenolic hydroxyl substituent of 8-hydroxyquinolinato unit in the formation of the Eu(III) complex. However, carbonyl group C=O directly linking with aromatic group may be favorable of enolizing under the present experimental conditions, so as to form a larger conjugated and a lower energy system, than the non-aromatic group such as –NH_2 when binding to metal ion and forming a complex [25]. It is the enolization and deprotonation of O=C–NH– group changing into $^-$O–C=N– that the $[HoL^1(NO_3)(DMF)_2]_2$ complex is of neutral charge and non-electrolyte, but both of $[YL(NO_3)(DMF)_2]_2Cl_2{\cdot}2(DMF)$ and $[LaL(NO_3)(MeOH)_2]_2(NO_3)_2$ complexes are of electrolytes. The enolization and deprotonation will afford an efficient route for investigators to design favorable molecules well.

*2.2.2. The crystal structure of complex **2d***

The unitary nine-coordination structure of the binuclear $3[HoL^4(NO_3)(DMF)_2]_2{\cdot}7(DMF)$ complex with a 1:1 metal-to-ligand stoichiometry is shown in Fig. 1B by the coordination sphere of ORTEP diagram (30% probability ellipsoids). Similarly, ligand **1d** acts as a dibasic tetradentate ligand, binding to Ho(III) through the phenolate oxygen atom, nitrogen atom of quinolinato unit and the C=N group, $^-$O–C=N– group (enolized and deprotonated from O=C–NH–) of the isonicotinylhydrazine side chain. Also, one DMF molecule is binding orthogonally to the ligand-plane from one side to the metal ion while another DMF and nitrate (bidentate) are binding from the other. Dimerization of the monomeric unit of one molecule occurs through the phenolate oxygen atoms leading to a central planar four-membered $(HoO)_2$ ring with the Ho···Ho separation of 3.936 Å. At the dimerization sites, the "set off" of the two parallel "HoL^4-planes" by 1.696 Å takes place. The distance between the two parallel ML-planes and the distance between M···M′ (in Table 2) may result from the size of M^{3+} and substituent effects simultaneously. Moreover, the O=C–NH– group of the isonicotinylhydrazine side chain has enolized and deprotonated into $^-$O–C=N– with the $^-$O–C and N=C band lengths being 1.283(5) and 1.311(6) Å, respectively.

2.3. Structural analysis for powder metal complexes

2.3.1. Elemental analysis and molar conductance

All the Ho(III) complexes are of orange powders, stable in air, and soluble in DMF and DMSO, but slightly soluble in methanol, ethanol, acetonitrile, ethyl acetate and acetone, THF and $CHCl_3$. The melting points of all the Ho(III) complexes exceed 300 °C. Elemental analyses indicate that all the Ho(III) complexes are of 1:1 metal-to-ligand (stoichiometry) complexes, and the data of molar conductance of the Ho(III) complexes in DMF solutions indicate that all of them act as non-electrolytes [26].

2.3.2. Infrared spectrum study

The characteristic IR spectrum bands (ν_{max}/cm^{-1}) of all the ligands showed $3576–3320_{vs}$ assigned to ν(NH); $1682–1643_s$ assigned to ν(CO) of the carbonyl groups of aroylhydrazine side chains and 1632–1602 assigned to ν(CN) of azomethines, whereas

Table 2
Comparison of the structural parameters of ligand L–H [10], ligand **1b** and **1d** when binding to different metal centers.

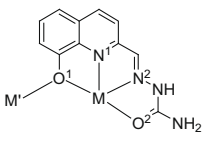

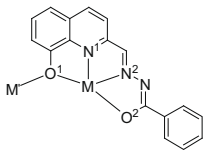

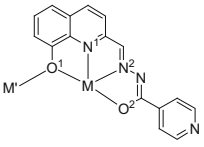

	$[LY(NO_3)(DMF)_2]_2Cl_2{\cdot}2(DMF)$	$[LLa(NO_3)(MeOH)_2]_2(NO_3)_2$	$[HoL^1(NO_3)(DMF)_2]_2$	$3[HoL^4(NO_3)(DMF)_2]_2{\cdot}7(DMF)$
O1–M	2.346(3)	2.425(3)	2.4072(18)	2.387(2)
N1–M	2.470(3)	2.541(3)	2.464(2)	2.464(3)
N2–M	2.563(4)	2.620(4)	2.526(2)	2.513(3)
O2–M	2.355(3)	2.414(3)	2.312(2)	2.333(3)
O1–M′	2.354(3)	2.387(3)	2.3729(17)	2.378(2)
O1–M–N1	66.8(1)	65.5(1)	66.07(7)	66.54(9)
N1–M–N2	61.4(1)	60.4(1)	62.64(8)	62.81(10)
N2–M–O2	63.1(1)	60.9(1)	62.52(8)	62.92(11)
Distance between the two parallel ML-planes	1.887	1.388	1.615	1.696
Distance between M···M′	3.886	3.980	3.990	3.936

1706_s assigned to ν(CO) of the formyl disappeared. Moreover, $3318–3139_{br}$ and $1288–1267_s$ should be assigned to ν(OH) and ν(C–OH) of the phenolic hydroxyl substituents, respectively, and 1581–1532 should be assigned to ν(CN) of pyridines.

Carefully compared with the characteristic IR bands of ligands, it comes to the conclusion that: (1) All the complexes show $3452–3389_{br}$ assigned to ν(OH) of H_2O; $974–935_w$ assigned to ρ_r (H_2O) and $650–611_w$ assigned to ρ_w (H_2O), indicating that there are coordinated water molecules participating in the Ho(III) complexes [27,28]. (2) All the complexes show 1106–1101 assigned to ν(C–OM), indicating that the binding of metal ion to every ligand through an O–M coordination linkage may take place [29]. (3) $3318–3139_s$ assigned to ν(OH) and 1288–1267 assigned to ν(C–OH) of the phenolic hydroxyl substituent of ligands have disappeared, but the new bands of 3192_s and 1248_s can be, respectively, assigned to ν(OH) and ν(C–OH) of the phenolic hydroxyl substituent of 2-hydroxybenzoylhydrazine side chain of **2b** complex, while the new bands of 3183_s and 1290_s can also be, respectively, assigned to ν(OH) and ν(C–OH) of the phenolic hydroxyl substituent of 4-hydroxybenzoylhydrazine side chain of **2c** complex. (4) $1682–1643_s$ assigned to ν(CO) and $3576–3320_{vs}$ assigned to ν(NH) of aroylhydrazine side chains of ligands have disappeared in all the IR spectra of Ho(III) complexes, indicating that they participate in the Ho(III) complexes with the groups of O=C–NH– of aroylhydrazine side chains enolizing and deprotonating into $^-$O–C=N– as proved by the above crystal structural analyses. (5) 1635–1599 assigned to ν(CN) of azomethines of the Ho(III) complexes have shifted by 33–6 cm^{-1} in comparison with bands of ligands, indicating that the nitrogen atoms of azomethines participate in the complexes. (6) 1571–1544 assigned to ν(CN) of pyridines of the Ho(III) complexes have shifted by 39–8 cm^{-1} in comparison with bands of ligands, indicating that the nitrogen atoms of pyridines also participate in the complexes. However, the new band of 1593 can be assigned to ν(CN) of free pyridine of isonicotinylhydrazine side chain of **2d** complex. (7) $591–590_w$ assigned to ν(MO) and $492–484_w$ assigned to ν(MN) of the Ho(III) complexes further indicate that oxygen atoms and nitrogen atoms participate in Ho(III) complexes. (8) All the Ho(III) complexes show 1497–1488 (ν_1), 1314–1308 (ν_4), 1065–1030 (ν_2), 815–802 (ν_3), 765–739 (ν_5), and $\Delta\nu(\nu_1–\nu_4)$ = 187–176 cm^{-1}, indicating that nitrate ions bidentately participate in the Ho(III) complexes [30].

The above results of elemental analyses, molar conductance and IR spectra indicate that the suggested compositions of the powder metal complexes are of $[HoL^{1–4}(NO_3)(H_2O)_2]_2$. In addition, the ESI-MS data in DMF solution (Supplementary material Fig. S1) for complex **2a** show that *m/z* data are 1324.3 $[M]^+$, 662.4 $[M/2]^+$ and 292.1 $[H_2L^1+H]^+$; for **2b**, the *m/z* 1357.6 $[M]^+$, 678.5 $[M/2]^+$ and 308.1 $[H_2L^2+H]^+$; for **2c**, the *m/z* 1358.7 $[M+H]^+$, 678.9 $[M/2]^+$ and 308.2 $[H_2L^3+H]^+$; for **2d**, the *m/z* 1326.7 $[M]^+$, 665.3 $[M/2+H]^+$ and 293.1 $[H_2L^4+H]^+$, indicating that the four coordinated water molecules for every powder binuclear Ho(III) complex can be replaced by four DMF molecules in DMF solution, and that the compositions of binuclear complexes in DMF solutions are of $[HoL^{1–4}(NO_3)(DMF)_2]_2$. However, besides binuclear structures, there are monomers in DMF solutions as shown by the ESI-MS data.

2.4. DNA binding properties

2.4.1. Viscosity titration measurements

Viscosity titration measurements were carried out to clarify the interaction modes between the investigated compounds and CT-DNA. Viscosity measurements are very sensitive to changes in the length of DNA, as viscosity is proportional to L^3 for rod-like DNA of length L. Intercalation involves the insertion of a planar molecule between DNA base pairs, which results in a decrease in the DNA helical twist and lengthening of the DNA, therefore intercalators cause the unwinding and lengthening of DNA helix as base pairs become separated to accommodate the binding compound [31,32]. Whereas, agents bound to DNA through groove binding do not alter the relative viscosity of DNA, and agents electrostatically bound to DNA will bend or kink the DNA helix, reducing its effective length and its viscosity, concomitantly [33,34]. The effects of ligands and Ho(III) complexes on the viscosities of CT-DNA are shown in Fig. 2. With the ratios of the investigated compounds to DNA (bps) increasing, the relative viscosities of DNA increase steadily, indicating that there exist intercalations between all the ligands and Ho(III) complexes with DNA helix. The crystal and other structural analyses show that all the Ho(III) complexes have two parallel planes, which may well be an indicator of the intercalation behaviour of these complexes binding to DNA helix. In addition, although there is a blend at lower molar concentration ratios of complexes to DNA, the relative viscosities of DNA increase with the order of **1a** > **1b** > **1c** > **1d** for ligands, the order of **2a** > **2b** > **2c** > **2d** for Ho(III) complexes, and the orders of **2a** > **1a**, **2b** > **1b**, **2c** > **1c** and **2d** > **1d**. These orders suggest the extents of the unwinding and lengthening of DNA helix by compounds and the affinities of compounds binding to DNA, which may be due to the key roles of substituent effects and the larger coplanar structures of Ho(III) complexes than those of ligands. Intercalation has been traditionally associated with molecules containing fused bi/tricyclic ring structures, though atypical intercalators with non-fused rings systems may be more prevalent than previously recognized [35]. So it is logical that all the large coplanar Ho(III)

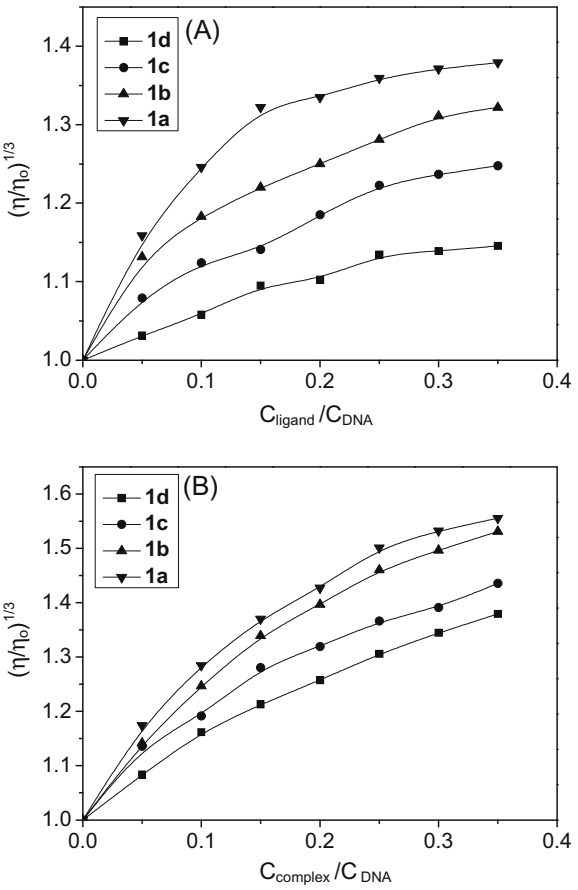

Fig. 2. Effects of increasing amounts of the investigated compounds on the relative viscosity of CT-DNA in 5 mmol Tris–HCl buffer solution (pH 7.20) containing 50 mmol NaCl at 25.00 ± 0.01 °C. Plots of (A) and (B) represent the ligands–CT-DNA and Ho(III) complexes–CT-DNA systems, respectively. The concentration of CT-DNA was 50 μM (bps).

complexes containing fused multiple cyclic ring structures and all the ligands containing fused bicyclic ring structures can bind to DNA through intercalations.

2.4.2. Ultraviolet–visible (UV–Vis) spectroscopy study

The UV–Vis absorption spectra of the investigated compounds in the absence and in the presence of the CT-DNA were obtained in DMF:Tris–HCl buffer (5 mmol, pH 7.20) containing 50 mmol NaCl of 1:100 solutions, respectively. The UV–Vis spectra values of the maximum absorption wavelength (λ_{max}), the molar absorptivity (ε) and the hypochromicity at λ_{max} for ligands and Ho(III) complexes are listed in Table S3 (see Supplementary material Table S3). The UV–Vis spectra of ligands have two types of absorption bands at λ_{max} in the regions of 290–300 nm (ε = 2.86–3.55 × 10^4 M^{-1} cm^{-1}) and 323–329 nm (ε = 1.78–2.36 × 10^4 M^{-1} cm^{-1}), which can be assigned to π–π* transitions within the organic molecules, and π–π* of the C═N and C═O groups, respectively. While the UV–Vis spectra of Ho(III) complexes have two types of absorption bands at λ_{max} in the regions of 326–336 nm (ε = 3.41–4.86 × 10^4 M^{-1} cm^{-1}) and 372–378 nm (ε = 3.18–3.94 × 10^4 M^{-1} cm^{-1}), which can be, respectively, assigned to π–π* transitions of the larger conjugated organic molecules and π–π* of the C═N–N═C groups coupled with charge transfers from ligands to metal ions ($L \rightarrow Ho^{3+}$) [27,28]. The band shifts of λ_{max} and the changes of ε for complexes in comparison with ligands indicate the formations of the Ho(III) complexes.

Upon successive additions of CT-DNA (bps), the UV–Vis absorption bands of ligand **1a**, **1b**, **1c** and **1d** show a progressive hypochromism of 34.3% at 295 nm, 30.1% at 294 nm, 22.5% at 300 nm and 8.4% at 290 nm by approximately saturated titration end points at C_{DNA}:C_{ligand} = 1.4–2.2:1, respectively, with a 1, 3, 1 and 0 nm red shifts of absorption bands in the region of 290–300 nm. Ligand **1a**, **1b**, **1c** and **1d** show another progressive hypochromism of 11.1% at 323 nm, 18.1% at 329 nm, 4.8% at 326 nm and 1.0% at 325 nm, respectively, with a 1, 3, 1 and 0 nm blue shifts in the region of 323–329 nm. Similarly, upon successive additions of CT-DNA (bps), the UV–Vis absorption bands of metal complex **2a**, **2b** and **2c** show a progressive hypochromism of 28.4% at 326 nm, 27.0% at 328 nm and 24.2% at 336 nm by approximately saturated titration end points at C_{DNA}:$C_{complex}$ = 1.4:1, respectively. Complex **2a**, **2b** and **2c** show another progressive hypochromism of 26.5% at 372 nm, 26.1% at 377 nm and 22.3% at 378 nm, respectively, but all of them show no band shift. Complex **2d** show two types of slightly unsteady hypochromisms of 0.38% at 328 nm and 2.32% at 372 nm by an approximately saturated titration end point at C_{DNA}:$C_{complex}$ = 1.4:1. There is no band shift for metal complexes apart from 1 nm blue shift for complex **2c**. In addition, isosbestic points at 342–357 nm for ligands and at 408–425 nm for Ho(III) complexes are observed, indicating that the reaction between every investigated compound and DNA takes places by an equilibrium. Absorption titration can monitor the interaction of a compound with DNA. The obvious hypochromism and red shift are usually characterized by the non-covalently intercalative binding of compound to DNA helix, due to the strong stacking interaction between the aromatic chromophore of the compound and base pairs of DNA [36,37]. However, the intercalation between a compound and DNA helix can not be excluded only by no or small red shift of UV–Vis absorption bands [38]. In fact, some groove binders of Hoechst 33 258 family can also present red shifts or even blue shifts of absorption bands when they bind to DNA helix by groove binding modes, especially for multiple binders [39,40]. After all, hydrodynamic measurements that are sensitive to length change of DNA (*i.e.*, viscosity and sedimentation) are regarded as the least ambiguous and the most critical criterions for binding modes in solution in absence of crystallographic structural data [41,42].

On the other hand, the magnitude of hypochromism is parallel to the intercalative strength and the affinity of a compound binding to DNA [43]. The appreciable hypochromisms of ligands and Ho(III) complexes intercalating to DNA present the order of **1a** > **1b** > **1c** > **1d** and the order of **2a** > **2c** > **2b** > **2d**. Apart from a slight blend for **2c** and **2d**, these orders are consistent with the viscosity titration results. Here, the substituent effects may play key roles in the interactions. As for complex **2a**, the phenyl substituent may be more accessible to DNA helix and much favorable of forming π–π stacking interaction between the aromatic chromophore of the complex and the base pairs of DNA than 2-hydroxyphenyl and 4-hydroxyphenyl subsituents of **2b** and **2c** complexes. As for complex **2d**, *N* atom of aromatic sextet of the pyridine ring of isonicotinylhydrazine side chain has an exposed and non-hybridized *p* orbital containing two long-pair electrons, which is orthogonal to conjugated π–π plane of the pyridine ring. This may result in a strong electron repulsion and hinder the π–π stacking interaction between the aromatic heterocyclic chromophore of the complex and the base pairs of DNA. Moreover, the aggregation of self-stacked molecules of **2d** complex may occur, which will induces the possibility of an association/dissociation equilibrium in the absence of DNA, and induces a slightly unsteady UV–Vis absorption and a little hypochromism even in an excess of conjugate vs. DNA bps [40]. As for the order of hypochromicity for ligands, it may be due to the same reasons as the metal complexes. Difference between them is that no significant aggregation of self-stacked molecules of ligand **1d** may occur unlike complex **2d**.

2.4.3. DNA–EtBr quenching assay

The fluorescence emission intensity of DNA–EtBr system decreased dramatically upon the increasing amounts of every ligand and Ho(III) complex. Stern–Volmer equation was used to determine the fluorescent quenching mechanism [31]. Plots of F_o/F vs. *[Q]* are shown in Fig. 3 and the quenching data collected and calculated from the good linear relationship when $P < 0.05$ are listed in Table 3. As shown, the data of K_{SV} are 1.405–3.016 × 10^4 M^{-1} for ligands and 3.796–16.50 × 10^4 M^{-1} for Ho(III) complexes, accordingly, the data of K_q calculated are 0.7806–1.676 × 10^{13} M^{-1} s^{-1} for ligands and 2.109–9.167 × 10^{13} M^{-1} s^{-1} for Ho(III) complexes, respectively, when the value of τ_o is taken as 1.8 × 10^{-9} s [31]. All of the current values of K_q for ligands and Ho(III) complexes are much greater than that of $K_{q(max)}$ (2.0 × 10^{10} M^{-1} s^{-1}), the maximum quenching rate constant of bimolecular diffusion collision, which are indicative of static types of quenching mechanisms arisen from the formations of dark complexes between the fluorophores and quenching agents [44,45]. It is reported that the loss of fluorescence intensity at the maximum wavelength indicates the displacement of EtBr from DNA–EtBr complex by a compound and the intercalative binding between the compound with DNA [34]. The DNA–EtBr quenching results also indicate that most of the EtBr molecules have been displaced from DNA–EtBr complex by every quencher by the approximately saturated end point. Thus, it is reasonable that there exist intercalations between DNA and these investigated compounds.

Additionally, The Stern–Volmer dynamic quenching constants can also be interpreted as binding affinities of the complexation reactions [46,47]. The data of K_{SV} present the order of **1c** > **1b** > **1a** > **1d** for ligands, the order of **2c** > **2b** > **2a** > **2d** for metal complexes, and the orders of **2a** > **1a**, **2b** > **1b**, **2c** > **1c**, **2d** > **1d**, which indicate the abilities of displacement of EtBr from DNA–EtBr systems by compounds and the binding affinities between compounds and DNA. However, the orders are not slightly in good agreement with the viscosity titration and UV–vis spectroscopy study results. Here, the phenolic hydroxy groups that can bind to nucleotides or/and the sugar–phosphate backbone of DNA through hydrogen bonds may play some roles in the DNA–EtBr quenching

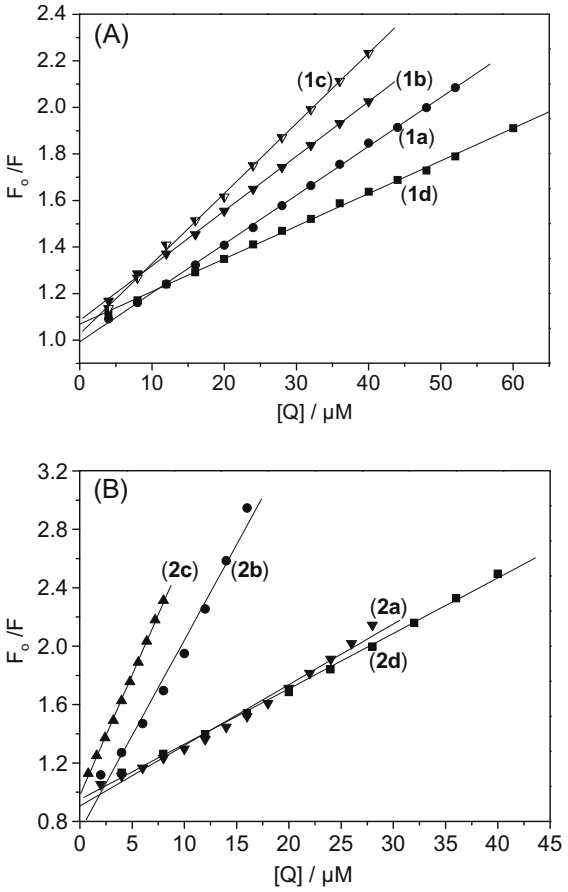

Fig. 3. Stern–Volmer plots of F_o/F vs. *[Q]* for ligands (A) and Ho(III) complexes (B). Tests were performed in the conditions of 5 mmol Tris–HCl buffer containing 50 mmol NaCl at 298 K. C_{DNA} = 4 μM (nucleotides), C_{EtBr} = 0.32 μM; λ_{ex} = 525 nm, λ_{em} = 587 nm.

tests. However, the other weak interactions such as hydrophobic force, Van der Waals force and electrostatic force (pH at 7.20) may not be excluded. In other words, the interaction mechanism is not only determined by complex formation but also by some weak interactions [48].

More importantly, DNA intercalators have been used extensively as antitumor, antineoplastic, antimalarial, antibiotic, and antifungal agents [31]. There is a criterion for screening out antitumor drugs from others by DNA–EtBr fluorescent tracer method, *i.e.*, a compound can be used as potential antitumor drug if it cause a 50% loss of DNA–EtBr fluorescence intensity by fluorescent titrations before the molar concentration ratio of the compound to DNA (nucleotides) does not overrun 100:1 [49]. CF_{50} value is introduced to denote the molar concentration of a compound that causes a 50% loss in the fluorescence intensity of DNA–EtBr system. According to the data of CF_{50} and the molar ratios of compounds to DNA shown in Table 3, it is interesting that at CF_{50}, all the molar concentration ratios of the investigated compounds to DNA (1.549–16.58:1) are largely under 100:1, indicating that all these ligands and Ho(III) complexes can be used as potential antitumor drugs, and the antitumor activities of Ho(III) complexes may be better than those of ligands. However, their pharmacodynamical, pharmacological and toxicological properties should be further studied *in vivo*.

2.4.4. Fluorescence spectroscopy study

When exited at λ_{ex} = 321–325 nm, ligands showed the fluorescence maximum wavelengths at λ_{em} = 429–444 nm, and exited at λ_{ex} = 331–334 nm the Ho(III) complexes showed the fluorescence maximum wavelengths at λ_{em} = 415–425 nm, respectively. Upon additions of DNA, the fluorescence emission intensity of every investigated compound grew steadily. Although the emission enhancement can not be regarded as a rigid criterion for binding mode, it is related to the extent to which the compound gets into a hydrophobic environment inside DNA and avoids the effect of solvent water molecules. To compare quantitatively the affinities of these compounds bound to DNA, the intrinsic binding constants K_b can be obtained by the fluorescence titration methods and Scatchard equation [34,50]. Scatchard plot should be a straight line for a simple binding reaction [51]. Because of the significant neighbour exclusion property of DNA binding to intercalating agents, the Scatchard plot of r/C_f vs. r usually presents a deviation from linearity [52]. As shown in Fig. S2 (see Supplementary material Fig. S2), every plots of r/C_f vs. r for ligands and Ho(III) complexes show deviation from linearity, so the binding constant was obtained by McGhee and von Hippel model [52,53]. The data of binding constants (K_b) and the moles of compound bound per mol of base pair of DNA ($1/n$) are shown in Table 3. The data of binding constants (K_b) present 10^5 M^{-1} with the order of **1b** > **1c** > **1a** > **1d** for ligands, which is slightly different from the order of DNA–EtBr quenching result. But the data of binding constants (K_b) present 0.1422–2.559 × 10^6 M^{-1} with the order of **2c** > **2b** > **2a** > **2d** for complexes, and orders of **2a** > **1a**, **2b** > **1b**, **2c** > **1c**, **2d** > **1d**, which are consistent with the orders of DNA–EtBr quenching results. Moreover, The binding constant (K_b) of EtBr to CT-DNA studied as the same methods and the same conditions of the investigated compounds present the order of magnitude at 3.166(±0.145) × 10^6 M^{-1} ($1/n$ = 0.24) in our laboratory (see Supplementary material Fig. S2 (I), which is consistent with the previous study result (EtBr–DNA, K_b = 3.0 × 10^6 M^{-1} in 5 mmol Tris–HCl/50 mmol NaCl buffer, pH = 7.2), indicating that **2b** (K_b = 2.373 × 10^6 M^{-1}) and **2c** (K_b = 2.559 × 10^6 M^{-1}) complexes can bind to DNA effectively [54].

Table 3
Parameters of K_b, K_{SV}, K_q, CF_{50}, IC_{50} (OH· and O_2^{-}·) for ligands (**1a–d**) and the Ho(III) complexes (**2a–d**) ($P < 0.05$).

Compound	$K_b \times 106$ M^{-1}	$1/n$[a]	$K_{SV} \times 10^4$ M^{-1} (*R*)	$K_q \times 10^{13}$ M^{-1} s^{-1}	CF_{50}[b] (μM) ($C_{compound}/C_{DNA,\ nucleotides}$)	IC_{50}[c] ±SD (μM) for OH· (*R*)	IC_{50}[c] ±SD (μM) for O_2^{-}· (*R*)
1a	0.2148 ± 0.0205	0.081	2.086 ± 0.014 (0.9997)	1.159	48.18 (12.05)	14.66 ± 0.495 (0.9937)	6.831 ± 0.219 (0.9954)
1b	0.9295 ± 0.1315	0.28	2.352 ± 0.018 (0.9998)	1.307	38.95 (9.738)	7.716 ± 0.230 (0.9940)	4.308 ± 0.174 (0.9892)
1c	0.7599 ± 0.0867	0.066	3.016 ± 0.027 (0.9997)	1.676	32.29 (8.073)	11.38 ± 0.441 (0.9902)	4.096 ± 0.112 (0.9955)
1d	0.1329 ± 0.0180	0.092	1.405 ± 0.013 (0.9995)	0.7806	66.30 (16.58)	76.10 ± 0.372 (0.9909)	5.131 ± 0.258 (0.9838)
2a	0.6519 ± 0.1023	0.28	4.156 ± 0.142 (0.9931)	2.309	26.36 (6.589)	2.253 ± 0.051 (0.9854)	8.024 ± 0.405 (0.9900)
2b	2.373 ± 0.319	0.20	13.07 ± 0.704 (0.9914)	7.261	9.683 (2.421)	1.869 ± 0.038 (0.9864)	11.38 ± 0.597 (0.9909)
2c	2.559 ± 0.684	0.22	16.50 ± 0.192 (0.9995)	9.167	6.198 (1.549)	1.286 ± 0.026 (0.9800)	26.92 ± 1.311 (0.9949)
2d	0.1422 ± 0.0145	0.13	3.796 ± 0.006 (0.9991)	2.109	27.69 (6.922)	3.615 ± 0.075 (0.9918)	6.639 ± 0.297 (0.9917)

[a] The data of $1/n$ represent moles of compound/mol of base pair of DNA.
[b] CF_{50} represents the molar concentration of the tested compound that causes a 50% loss in the fluorescence intensity of EtBr–DNA system.
[c] IC_{50} value was calculated from regression line of the log of the tested compound concentration vs. the scavenging effect (%) of the compound. *R* represents the linear correlation coefficient.

2.5. Antioxidation

2.5.1. Hydroxyl radical scavenging activity

Fig. 4A and B show the plots of hydroxyl radical scavenging effect (%) for ligands and Ho(III) complexes, respectively, which are concentration-dependant. As shown in Table 3, the values of IC_{50} of ligands for hydroxyl radical scavenging effect are 7.716–76.10 μM with the order of **1b** < **1c** < **1a** < **1d**, while the values of IC_{50} of Ho(III) complexes for hydroxyl radical scavenging effect are 1.286–3.615 μM with the order of **2c** < **2b** < **2a** < **2d**. These orders of IC_{50} are opposite to the abilities of scavenging effects for hydroxyl radicals. It is marked that the hydroxyl radical scavenging effects of Ho(III) complexes are much higher than those of their ligands, possibly in that the larger conjugated metal complexes can react with HO· to form larger stable macromolecular radicals than ligands [55]. Moreover, ligand **1b**, **1c** and their Ho(III) complexes show higher abilities of scavenging effects for hydroxyl radicals than other ligands and Ho(III) complexes, possibly due to the key roles of functional groups, –OH, which can react with HO· to form stable macromolecular radicals by the typical H-abstraction reaction [55]. Furthermore, for hydroxyl radical, there are two types of antioxidation mechanisms, in which one presents suppression of the generation of the hydroxyl radicals, and another presents scavenging of the hydroxyl radicals generated [55]. Hydroxyl radical production, detected by ethylene formation from methional, has been investigated in plasma, lymph and synovial fluid in the previous study [56]. In the presence of iron–EDTA as a catalyst, addition of either H_2O_2 or xanthine and xanthine oxidase give rise to hydroxyl radical formation that in most cases is not superoxide-dependent. In the absence of iron–EDTA, the reaction is hardly detectable, the rate being less than 5% of that observed with 1 μM iron–EDTA added. In the present study, the chelation between phenolic hydroxyl group and carbonyl group of 2-hydroxybenzoylhydrazine side chain for ligand **1b** with free Fe^{2+} in iron–EDTA reaction system may make the concentration of free Fe^{2+} much lower so that the catalysis becomes very poor and the hydroxyl radical formation has been suppressed, thus, the inhibitive effect of **1b** detected for hydroxyl radical is higher than those of other ligands. However, after formation of Ho(III) complex, the chelation between **1b** and free Fe^{2+} may be destroyed with the formation of intramolecular hydrogen bands for **2b**, so the hydroxyl radical scavenging effect (%) of **2b** is slightly lower than that of complex **2c**.

2.5.2. Superoxide radical scavenging activity

Fig. 4C and D show the plots of superoxide radical scavenging effect (%) for ligands and Ho(III) complexes, respectively, which are also concentration-dependant, but both the lines slightly blend together. As shown in Table 3, the values of IC_{50} of ligands for superoxide radical scavenging effects are 4.096–6.831 μM with no significant difference from each other, but the values of IC_{50} of Ho(III) complexes for superoxide radical scavenging effects are 6.639–26.92 μM with a notably different order of **2d** < **2a** < **2b** < **2c**. These results suggest that there are different mechanisms

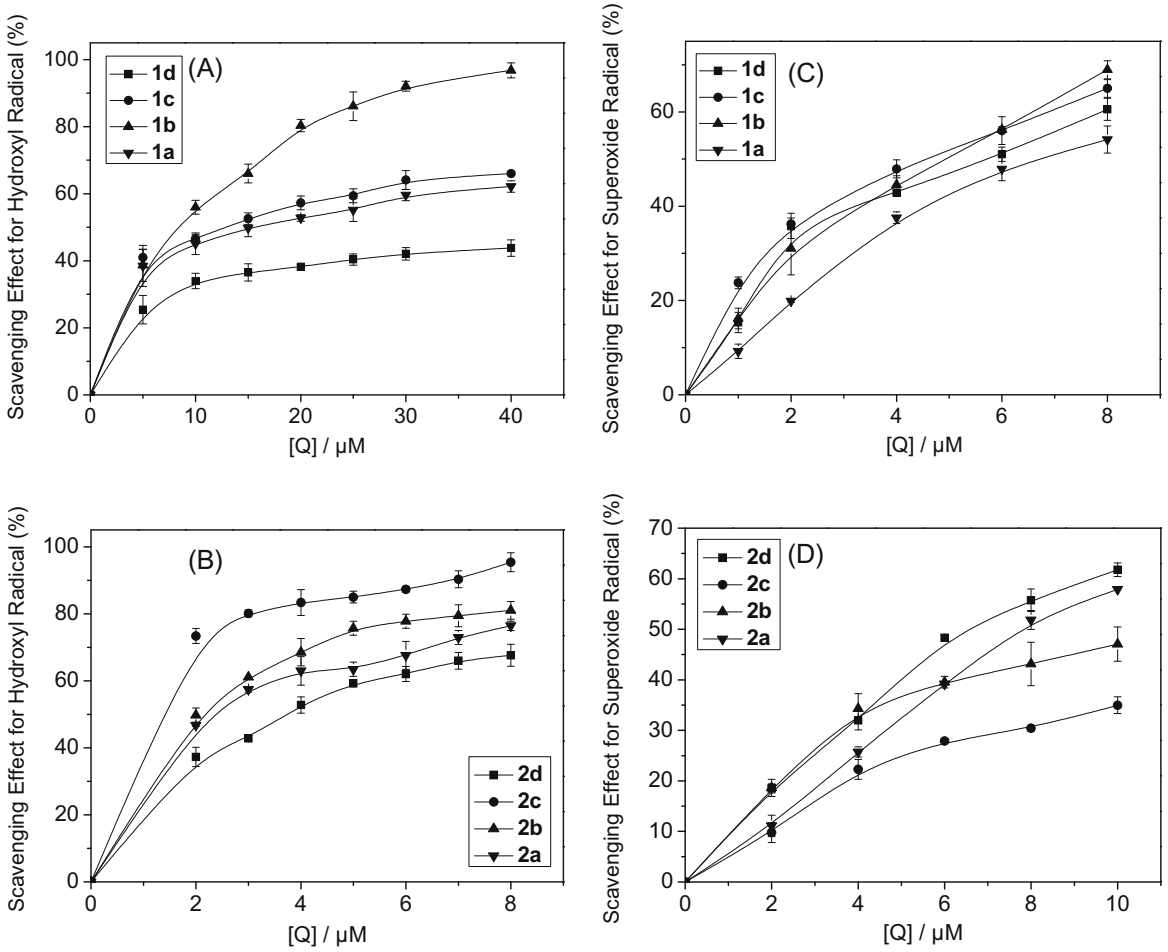

Fig. 4. Plots of antioxidation properties for ligands and Ho(III) complexes. (A) and (B) represent the hydroxyl radical scavenging effect (%) for ligands and Ho(III) complexes, respectively. (C) and (D) represent the superoxide radical scavenging effect (%) for ligands and Ho(III) complexes, respectively.

between scavenging or inhibiting hydroxyl radicals and superoxide radicals, which should be further studied.

It is reported that the value of IC_{50} of ascorbic acid (Vc), a standard agent for non-enzymatic reaction, for hydroxyl radicals is 1.537 mg ml^{-1} (8.727 mmol), and the scavenging effect of Vc for superoxide radicals is only 25% at 1.75 mg ml^{-1} (9.94 mmol) [57]. It is pronounced that all the ligands and the Ho(III) complexes investigated here have much stronger scavenging abilities for hydroxyl radicals and superoxide radicals than ascorbic acid (Vc). Endowed with antioxidative properties, these DNA binders may be effective inhibitors of the formation of a DNA/TBP complex topoisomerases [21–23].

3. Conclusion

The Ho(III) complexes are prepared from $Ho(NO_3)_3{\cdot}6H_2O$ and Schiff-base ligands derived from 8-hydroxyquinoline-2-carboxyaldehyde with four aroylhydrazines including benzoylhydrazine, 2-hydroxybenzoylhydrazine, 4-hydroxybenzoylhydrazine and isonicotinylhydrazine, respectively. X-ray crystal and other structural analyses show that Ho(III) and every ligand can form a binucleae Ho(III) complex with a 1:1 metal-to-ligand stoichiometry by nine-coordination at the Ho(III) center. Every ligand acts as a dibasic tetradentate ligand, binding to Ho(III) through the phenolate oxygen atom, nitrogen atom of quinolinato unit and the C=N group, $^{-}$O–C=N– group (enolized and deprotonated from O=C–NH– group) of the aroylhydrazine side chain. Dimerization of this monomeric unit occurs through the phenolate oxygen atoms leading to a central planar four-membered $(HoO)_2$ ring. It is the key roles of enolization and deprotonation of O=C–NH– group changing into $^{-}$O–C=N– of the aroylhydrazine side chain that the dimeric centronucleus of every Ho(III) complex is of neutral charge, which will afford an efficient route for investigators to well design favorable molecules. In addition, all the ligands and Ho(III) complexes can bind to CT-DNA through intercalations with the binding constants at 10^5–10^6 M^{-1}, but Ho(III) complexes present stronger affinities to DNA than ligands. DNA–EtBr fluorescent tracer methods show that all the ligands and Ho(III) complexes may be used as potential anticancer drugs but the antitumor activities of Ho(III) complexes may be better than those of ligands. However, their pharmacodynamical, pharmacological and toxicological properties should be further studied *in vivo*.

On the other hand, all the ligands and Ho(III) complexes have strong abilities of antioxidation for hydroxyl radicals and superoxide radicals but Ho(III) complexes show stronger scavenging effects for hydroxyl radicals than ligands. Whether Ho(III) complexes or ligands containing active phenolic hydroxy groups present stronger abilities of scavenging effects for hydroxyl radicals than others. Endowed with antioxidative properties, these DNA binders may be effective inhibitors of the formation of a DNA/TBP complex topoisomerases, which should be studied further *in vivo*. Moreover, the complex **2c** has lower ability of scavenging superoxide radicals than other complexes and the different mechanism between scavenging hydroxyl radicals and superoxide radicals should be also studied further.

4. Experimental

4.1. Materials

Calf thymus DNA (CT-DNA) and ethidium bromide (EtBr) were obtained from Sigma–Aldrich Biotech. Co., Ltd. 8-Hydroxyquinoline-2-carboxyaldehyde was obtained form J&K Chemical Co., Ltd. All the stock solutions (1.0 mmol) of the investigated compounds were prepared by dissolving the powder materials into appropriate amounts of DMF solutions, respectively. Deionized double distilled water and analytical grade reagents were used throughout. CT-DNA stock solution was prepared by dissolving the solid material, normally at 0.3 mg ml^{-1}, in 5 mmol Tris–HCl buffer (pH 7.20) containing 50 mmol NaCl. Then, the solution was kept over 48 h at 4 °C. The resulting somewhat viscous solution was clear and particle-free. The solution of CT-DNA in Tris–HCl buffer gave a ratio of UV–vis absorbance at 260 to 280 nm of about 1.8–1.9, indicating that the CT-DNA was sufficiently free of protein. The CT-DNA concentration in terms of base pair L^{-1} was determined spectrophotometrically by employing an extinction coefficient of ε = 13 200 M^{-1} cm^{-1} $(base\ pair)^{-1}$ at 260 nm. The CT-DNA concentration in terms of nucleotide L^{-1} was also determined spectrophotometrically by employing an extinction coefficient of 6600 M^{-1} cm^{-1} $(nucleotide)^{-1}$ at 260 nm [58]. The stock solution was stored at −20 °C until it was used. Working standard solution of CT-DNA was obtained by appropriate dilution of the stock solution in 5 mmol Tris–HCl buffer (pH 7.20) containing 50 mmol NaCl. EtBr was dissolved in 5 mmol Tris–HCl buffer (pH 7.20) and its concentration was determined assuming a molar extinction coefficient of 5600 L mol^{-1} cm^{-1} at 480 nm [31].

4.2. Methods

The melting points of the compounds were determined on an XT4-100X microscopic melting point apparatus (Beijing, China). Elemental analyses of C, N and H were carried out on an Elemental Vario EL analyzer. The metal ion content was determined by complexo-metric titration with EDTA after destruction of the complex in the conventional manner. The IR spectra were recorded on a Nicolet Nexus 670 FT-IR spectrometer using KBr disc in the 4000–400 cm^{-1} region. ^{1}H NMR spectra were recorded on a Bruker Advance DRX 200-MHz spectrometer with tetramethylsilane (TMS) as an internal standard. ESI-MS (ESI-Trap/Mass) spectra were recorded on a Bruker Esquire6000 Mass spectrophotometer and formic acid was used as the proton source. Ultraviolet–visible (UV–Vis) spectra were obtained using a Perkin–Elmer Lambda UV–Vis spectrophotometer.

Viscosity titration experiments were carried on an Ubbelohde viscometer in a thermostated water-bath maintained at 25.00 ± 0.01 °C. Titrations were performed for an investigated compound that was introduced into DNA solution (50 μM, bps) present in the viscometer. Data were presented as $(\eta/\eta_o)^{1/3}$ vs. the ratio of the compound to DNA, where η is the viscosity of DNA in the presence of the compound corrected from the solvent effect, and η_o is the viscosity of DNA alone. Relative viscosities for DNA in either the presence or absence of compound were calculated from the following relation:

$$\eta = (t - t_o)/t_o \quad (1)$$

where t is the observed flow time of the DNA containing solution, and t_o is the flow time of buffer [31,33].

Fluorescence spectra were recorded using RF–5301PC spectrofluorophotometer (Shimadzu, Japan) with a 1 cm quartz cell. Both of the excitation and emission band widths were 10 nm. All the experiments were measured after 5 min at a constant room temperature, 298 K. The intrinsic binding constants K_b could be obtained by the fluorescence titration methods and Scatchard equation [50]:

$$r/C_f = nK_b - rK_b \quad (2)$$

where r is the moles of compound bound per mole nucleotides of DNA; C_f is the molar concentration of free compound; n is the number of binding sites or the maximum number of compound bound per nucleotide; and K_b is the association or binding constant. C_f and r could be calculated according to the following equations [34]:

$$C_f = C_t - C_b \quad (3)$$

$$C_b = C_t(F - F_o)/(F_{max} - F_o) \quad (4)$$

$$r = C_b/C_{DNA} \quad (5)$$

where C_t is the total molar concentration of compound; C_b is the molar concentration of compound bound for DNA; F is the observed fluorescence emission intensity at a given DNA concentration C_{DNA} (nucleotides); F_o is the fluorescence emission intensity in the absence of DNA; and F_{max} is the maximum fluorescence emission intensity of the compound totally bound for DNA at a titration end point. The binding constants were also obtained by McGhee and von Hippel model [52,53]:

$$\frac{r}{C_f} = K_b(1 - nr)\left[\frac{1 - nr}{1 - (n-1)r}\right]^{n-1} \quad (6)$$

where K_b is the intrinsic binding constant and n is the exclusion parameter in DNA base pairs. The experimental parameters K_b and n were adjusted to produce curves that gave, by inspection, the most satisfactory fits to the experimental data.

DNA–EtBr quenching assay was performed as reported in a literature but with small changes [59]. DNA (4.0 μM, nucleotides) solution was added incrementally to 0.32 μM EtBr solution, until the rise in the fluorescence (λ_{ex} = 496 nm, λ_{em} = 596 nm) attained a saturation. Then, small aliquots of concentrated compound solutions (1.0 mmol) were added till the drop in fluorescence intensity (λ_{ex} = 525 nm, λ_{em} = 587 nm) reached a constant value. Measurements were made after 5 min at a constant room temperature, 298 K. Stern–Volmer equation was used to determine the fluorescent quenching mechanisms [31]:

$$F_o/F = 1 + K_q\tau_o[Q] = 1 + K_{SV}[Q] \quad (7)$$

where F_o and F are the fluorescence intensity in the absence and in the presence of a compound at *[Q]* concentration, respectively; K_{SV} is the Stern–Volmer dynamic quenching constant; K_q is the quenching rate constant of bimolecular diffusion collision; and τ_o is the lifetime of free EtBr.

The hydroxyl radicals in aqueous media were generated through the Fenton-type reaction [56,60]. The 5 ml reaction mixtures contained 2.0 ml of 100 mmol phosphate buffer (pH = 7.4), 1.0 ml of 0.10 mmol aqueous safranin, 1 ml of 1.0 mmol aqueous EDTA–Fe(II), 1 ml of 3% aqueous H_2O_2, and a series of quantitatively microadding solutions of the tested compound. The sample without the tested compound was used as the control. The reaction mixtures were incubated at 37 °C for 60 min in a water-bath. Absorbance at 520 nm was measured and the solvent effect was corrected throughout. The scavenging effect for $OH^{\cdot}$ was calculated from the following expression [34,61]:

$$\text{Scavenging effect } (\%) = \frac{A_{sample} - A_{blank}}{A_{control} - A_{blank}} \times 100 \quad (8)$$

where A_{sample} is the absorbance of the sample in the presence of the tested compound, A_{blank} is the absorbance of the blank in the absence of the tested compound and $A_{control}$ is the absorbance in the absence of the tested compound and EDTA–Fe(II).

The superoxide radicals ($O_2^{-\cdot}$) were produced by the MET–VitB_2–NBT system [34,61]. The solution of MET (methionine), VitB_2 (vitamin B_2) and NBT (nitroblue tetrazolium) were prepared with deionized double distilled water under lightproof conditions. The 5 ml reaction mixtures contained 2.5 ml of 100 mmol phosphate buffer (pH 7.8), 1.0 ml of 50 mmol MET, 1.0 ml of 0.23 mmol NBT, 0.50 ml of 33 μM VitB_2, and a series of quantitatively microadding solutions of the tested compound. After incubated at 30 °C for 10 min in a water-bath and then illuminated with a fluorescent lamp (4000 Lux), the absorbance of the sample was measured at 560 nm and the solvent effect was corrected throughout. The sample reaction mixtures without the tested compound were used as the control. The scavenging effect for $O_2^{-\cdot}$ was calculated from the following expression:

$$\text{Scavenging effect } (\%) = \frac{A_o - A_i}{A_o} \times 100 \quad (9)$$

where A_i is the absorbance in the presence of the tested compound and A_o is the absorbance in the absence of the tested compound.

The data for antioxidation presented as means ± SD of three determinations and followed by Student's *t*-test. Differences were considered to be statistically significant if $P < 0.05$. IC_{50} value was introduced to denote the molar concentration of the tested compound which caused a 50% inhibitory or scavenging effect on hydroxyl radicals or superoxide radicals.

4.3. Synthesis of ligands (**1a–d**)

4.3.1. 8-Hydroxyquinoline-2-carboxyaldehyde-(benzoyl)hydrazone (**1a**, H_2L^1)

Ligand **1a** was prepared by refluxing and stirring a 10 ml ethanol solution of 8-hydroxyquinoline-2-carboxadehyde (0.519 g, 3 mmol) and a 10 ml 90% ethanol aqueous solution of benzoylhydrazine (0.408 g, 3 mmol) for 8 h. After cooling to room temperature, the precipitate was filtered, recrystallized from 80% methanol aqueous solution and dried in vacuum over 48 h to give a pale yellow powder, yield 74.7% (0.656 g). M.p. = 221 °C. ESI-MS *m/z* 292.1 $[H_2L^1+H]^+$. ^{1}H NMR (DMSO-d_6, 200 MHz, TMS) δ: 8.637 (s, 1H, 11-CH=N), 8.343 (d, J = 8.8 Hz, 1H, 4-CH), 8.119 (d, J = 8.8 Hz, 1H, 3-CH), 7.936 (d, J = 6.4 Hz, 2H, 16,20-CH), 7.630–7.507 (m, 3H, 17,18,19-CH), 7.467–7.387 (m, 2H, 5,6-CH), 7.131 (d, 1H, J = 5.0 Hz, 7-CH). IR (KBr): 3359, 3318, 1682, 1602, 1546, 1267 cm^{-1}. UV–Vis (DMF/H_2O) λ_{max} (ε) = 295 (35 500), 323 nm (21 100 M^{-1} cm^{-1}).

In the same way as ligand **1a**, ligand **1b** (yellow precipitate), **1c** (pale yellow precipitate) and **1d** (yellow precipitate) were prepared from equimolar amounts of 8-hydroxyquinoline-2-carboxyaldehyde and 2-hydroxybenzoylhydrazine, 4-hydroxybenzoylhydrazine and isonicotinylhydrazine, respectively.

4.3.2. 8-Hydroxyquinoline-2-carboxyaldehyde-(2′-hydroxybenzoyl)-hydrazone (**1b**, H_2L^2)

Yield 81.0%. M.p. = 245–247 °C. ESI-MS *m/z* 308.1 $[H_2L^2+H]^+$. ^{1}H NMR (DMSO-d_6, 200 MHz, TMS) δ: 8.621 (s, 1H, 11-CH=N), 8.356 (d, J = 8.6 Hz, 1H, 4-CH), 8.113 (d, J = 8.6 Hz, 1H, 3-CH), 7.871 (d, 1H, J = 7.8 Hz, 20-CH), 7.469–7.395 (m, 3H, 5,6,18-CH), 7.133 (d, J = 7.0 Hz, 1H, 7-CH), 7.018–6.943 (m, 2H, 17,19-CH); IR (KBr): 3464, 3250, 1643, 1607, 1532, 1288 cm^{-1}. UV–Vis (DMF/H_2O) λ_{max} (ε) = 294 (31 600), 329 nm (23 600 M^{-1} cm^{-1}).

4.3.3. 8-Hydroxyquinoline-2-carboxyaldehyde-(4′-hydroxybenzoyl)-hydrazone (**1c**, H_2L^3)

Yield 81.0%. M.p. = 279–280 °C. ESI-MS *m/z* 308.2 $[H_2L^3+H]^+$. ^{1}H NMR (DMSO-d_6, 200 MHz, TMS) δ: 8.594 (s, 1H, 11-CH=N), 8.329 (d, J = 8.4 Hz, 1H, 4-CH), 8.088 (d, J = 8.4 Hz, 1H, 3-CH), 7.834 (d, 2H, J = 10.4 Hz, 16,20-CH), 7.493–7.379 (m, 2H, 5,6-CH), 7.124 (d, J = 6.8 Hz, 1H, 7-CH), 6.900 (d, J = 10.4 Hz, 2H, 17,19-CH). IR (KBr): 3320, 3139, 1660, 1632, 1581, 1277 cm^{-1}. UV–Vis (DMF/H_2O) λ_{max} (ε) = 300 (31 800), 326 nm (22 400 M^{-1} cm^{-1}).

4.3.4. 8-Hydroxyquinoline-2-carboxyaldehyde-(isonicotinyl)-hydrazone (**1d**, H_2L^4)

Yield 71.0%. M.p. = 162–164 °C. ESI-MS *m/z* 293.1 $[H_2L^4+H]^+$. ^{1}H NMR (DMSO-d_6, 200 MHz, TMS) δ: 8.813 (d, J = 5.2 Hz, 2 H, 17,19-CH), 8.657 (s, 1H, 11-CH=N), 8.372 (d, J = 8.8 Hz, 1H, 4-CH), 8.129 (d, J = 8.8 Hz, 1H, 3-CH), 7.861 (d, J = 5.2 Hz, 2H,

16,20-CH), 7.528–7.409 (m, 2H, 5,6-CH), 7.148 (d, J = 6.4 Hz, 1H, 7-CH). IR (KBr): 3576, 3193, 1663, 1613, 1557, 1271 cm^{-1}. UV–Vis (DMF/H_2O) λ_{max} (ε) = 290 (28 600), 325 nm (17 800 M^{-1} cm^{-1}).

4.4. Synthesis of metal complexes (**2a–d**)

4.4.1. Complex **2a**

Complex **2a** was prepared by refluxing and stirring equimolar amounts of a 40 ml methanol solution of ligand **1a** (0.058 g, 0.2 mmol) and $Ho(NO_3)\cdot 6H_2O$ on a water-bath. After refluxed for 30 min, triethylamine (0.020 g, 0.2 mmol) was added into the reaction mixtures dropwise to deprotonate the phenolic hydroxyl substituent of 8-hydroxyquinolinato unit. Then, the mixtures were refluxed and stirred continuously for 8 h. After cooling to room temperature, the precipitate was centrifugalized, washed with methanol and dried in vacuum over 48 h to give an orange powder, yield 87.3% (0.096 g); Anal. Calc. for $C_{34}H_{30}N_8O_{14}Ho_2$: C, 36.94; H, 2.72; N, 10.14; Ho, 29.87. Found: C, 37.03; H, 2.73; N, 10.00; Ho, 29.83%. ESI-MS (DMF solution) m/z 1324.3 $[M]^+$, 662.4 $[M/2]^+$, 292.1 $[H_2L^1+H]^+$; IR (KBr): 3452, 1608, 1556, 1492, 1309, 1105, 1035, 948, 812, 739, 614, 590, 492 cm^{-1}; UV–Vis (DMF/H_2O): λ_{max} (ε) = 326 (41 700), 372 nm (32 200 M^{-1} cm^{-1}); Λ_m (DMF) = 41.2 cm^2 Ω^{-1} mol^{-1}.

Similarly, complex **2b**, **2c** and **2d** were prepared from equimolar amounts of $Ho(NO_3)\cdot 6H_2O$ and **1b**, **1c** and **1d**, respectively.

4.4.2. Complex **2b**

Yield: 88.8%; Anal. Calc. for $C_{34}H_{30}N_8O_{16}Ho_2$: C, 35.90; H, 2.64; N, 9.85; Ho, 29.02. Found: C, 35.98; H, 2.64; N, 9.87; Ho, 28.94%. ESI-MS (DMF solution) m/z 1357.6 $[M]^+$, 678.5 $[M/2]^+$, 308.1 $[H_2L^2+H]^+$; IR (KBr): (cm^{-1}): 3389, 3192, 1615, 1571, 1497, 1310, 1271, 1101, 1030, 952, 815, 753, 650, 591, 484; UV–Vis (DMF/H_2O): λ_{max} (ε) = 326 (33 900), 375 nm (35 400 M^{-1} cm^{-1}). Λ_m (DMF) = 39.0 cm^2 Ω^{-1} mol^{-1}.

4.4.3. Complex **2c**

Yield: 90.2%; Anal. Calc. for $C_{34}H_{30}N_8O_{16}Ho_2$: C, 35.90; H, 2.64; N, 9.85; Ho, 29.02. Found: C, 36.12; H, 2.63; N, 9.87; Ho, 28.99%. ESI-MS (DMF solution) m/z 1358.7 $[M+H]^+$, 678.9 $[M/2]^+$, 308.2 $[H_2L^3+H]^+$; IR (KBr): (cm^{-1}): 3419, 3183, 1599, 1544, 1488, 1308, 1290, 1106, 1065, 974, 802, 765, 637, 590, 489; UV–Vis (DMF/H_2O): λ_{max} (ε) = 334 (48 700), 379 nm (41 400 M^{-1} cm^{-1}). Λ_m (DMF) = 39.9 cm^2 Ω^{-1} mol^{-1}.

4.4.4. Complex **2d**

Yield: 83.8%; Anal. Calc. for $C_{32}H_{28}N_{10}O_{14}Ho_2$: C, 34.70; H, 2.53; N, 12.65; Ho, 29.81. Found: C, 34.79; H, 2.52; N, 12.70; Ho, 29.90%. ESI-MS (DMF solution) m/z 1326.7 $[M]^+$, 665.3 $[M/2+H]^+$, 293.1 $[H_2L^4+H]^+$; IR (KBr): (cm^{-1}): 3396, 1635, 1593, 1549, 1490, 1314, 1102, 1057, 935, 814, 742, 611, 590, 492; UV–Vis (DMF/H_2O): λ_{max} (ε) = 326 (40 900), 371 nm (33 700 M^{-1} cm^{-1}). Λ_m (DMF) = 43.8 cm^2 Ω^{-1} mol^{-1}.

4.5. Determination of crystal structures

X-ray diffraction data for a crystal were performed with graphite-monochromated Mo Kα radiation (0.71073 Å) on a Bruker APEX area-detector diffractometer and collected by the ω–2θ scan technique at 296(2) K. The crystal structure was solved by direct methods. All non-hydrogen atoms were refined anisotropically by full-matrix least-squares methods on F^2. A partial structure was obtained by direct methods and the remaining non-hydrogen atoms were located from difference maps. All calculations were performed using the programs SHELXS-97 and SHELXL-97 [62].

Acknowledgements

The study was supported by the National Natural Science Foundation of China (20475023) and Gansu NSF (3ZS 041-A25-016).

Appendix A. Supplementary material

CCDC 715980 and 715981 contain the supplementary crystallographic data for this paper. These data can be obtained free of charge from The Cambridge Crystallographic Data Centre via www.ccdc.cam.ac.uk/data_request/cif. Supplementary data associated with this article can be found, in the online version, at doi:10.1016/j.jorganchem.2009.05.031.

References

[1] G. Zuber, J.C.J. Quada, S.M. Hecht, J. Am. Chem. Soc. 120 (1998) 9368–9369.
[2] V.S. Li, D. Choi, Z. Wang, L.S. Jimenez, M.S. Tang, H. Kohn, J. Am. Chem. Soc. 118 (1996) 2326–2331.
[3] Y.B. Zeng, N. Yang, W.S. Liu, N. Tang, J. Inorg. Biochem. 97 (2003) 258–264.
[4] A.M. Pyle, T. Morii, J.K. Barton, J. Am. Chem. Soc. 112 (1990) 9432–9434.
[5] J.K. Barton, J.M. Goldberg, C.V. Kumar, N.J. Turro, J. Am. Chem. Soc. 108 (1986) 2081–2088.
[6] S. Mahadevan, M. Palaniandavar, Inorg. Chim. Acre 254 (1997) 291–302.
[7] S.J. Lippard, Acc. Chem. Res. 11 (1978) 211–217.
[8] S.M. Hech, Acc. Chem. Res. 19 (1986) 383–391.
[9] D. Parker, R.S. Dickins, H. Puschmann, C. Crossland, J.A.K. Howard, Chem. Rev. 102 (2002) 1977–2010.
[10] M. Albrecht, O. Osetska, R. Fröhliich, Dalton Trans. 23 (2005) 3757–3762.
[11] R.B. Hunter, W. Walker, Nature 178 (1956) 47.
[12] D.M. Kramsch, A.J. Aspen, L.J. Rozler, Science 213 (1981) 1511–1512.
[13] E.M. Hodnett, P.D. Mooney, J. Med. Chem. 13 (1970) 786.
[14] E.M. Hodnett, W.J. Dunn, J. Med. Chem. 15 (1972) 339.
[15] L.H. Schmidt, Ann. Rev. Microbiol. 23 (1969) 427–454.
[16] A.A. El-Asmy, A.Z. El-Sonbati, A.A. Ba-Issa, M. Mounir, Transition Met. Chem. 5 (1990) 222–225.
[17] B.N. Ames, M.K. Shigenaga, T.M. Hagen, Proc. Natl. Acad. Sci. USA 90 (1993) 7915–7922.
[18] A.A. Horton, S. Fairhurst, Crit. Rev. Toxicol. 18 (1987) 27–29.
[19] H.L. Wang, Z.Y. Yang, B.D. Wang, Transition Met. Chem. 31 (2006) 470–474.
[20] S.F. Lo, V. Mulabagal, C.L. Chen, C.L. Kuo, H.S. Tsay, J. Agric. Food Chem. 52 (2004) 6916–6919.
[21] S.Y. Chiang, J. Welch, F.J. Rauscher, T.A. Beerman, Biochemistry 33 (1994) 7033–7040.
[22] J.M. Woynarowski, M. Mchugh, R.D. Sigmund, T.A. Beerman, Mol. Pharmacol. 35 (1989) 177–182.
[23] A.Y. Chen, C. Yu, B. Gatto, L.F. Liu, Proc. Natl. Acad. Sci. USA 90 (1993) 8131–8135.
[24] X.M. Chen, J.W. Cai, Single-Crystal Structural Analysis. Principles and Practices, Science Press, Beijing, 2003.
[25] Y.-C. Liu, Z.-Y. Yang, Biometals (2009), doi:10.1007/s10534-009-9221-8.
[26] W.J. Geary, Coord. Chem. Rev. 7 (1971) 81–122.
[27] M.M. Moawad, W.G. Hanna, J. Coord. Chem. 55 (2002) 439–457.
[28] T.M.A. Ismail, J. Coord. Chem. 58 (2005) 141–151.
[29] J.M. Ou-Yang, J. Inorg. Chem. (in Chinese) 13 (1997) 315–319.
[30] X.H. Lu, Q.Y. Lin, L.C. Kong, X.Q. He, Chem. Res. Appl. (in Chinese) 18 (2006) 1380–1385.
[31] D. Suh, J.B. Chaires, Bioorg. Med. Chem. 3 (1995) 723–728.
[32] R. Palchaudhuri, P.J. Hergenrother, Curr. Opin. Biotechnol. 18 (2007) 497–503.
[33] S. Satyanarayana, J.C. Dabrowiak, J.B. Chaires, Biochemistry 31 (1992) 9319–9324.
[34] B.D. Wang, Z.Y. Yang, P. Crewdson, D.Q. Wang, J. Inorg. Biochem. 101 (2007) 1492–1504.
[35] R.D. Snyder, Mutat. Res. 623 (2007) 72–82.
[36] J.K. Barton, A.T. Danishefsky, J.M. Goldberg, J. Am. Chem. Soc. 106 (1984) 2172–2176.
[37] H.L. Lu, J.J. Liang, Z.Z. Zeng, P.X. Xi, X.H. Liu, F.J. Chen, Z.H. Xu, Transition Met. Chem. 32 (2007) 564–569.
[38] Y.-C. Liu, Z.-Y. Yang, J. Inorg. Biochem. (2009), doi:10.1016/j.jinorgbio.2009.04.013.
[39] C. Behrens, N. Harrit, P.E. Nielsen, Bioconjugate Chem. 12 (2001) 1021–1027.
[40] S. Frau, J. Bernadou, B. Meunier, Bioconjugate Chem. 8 (1997) 222–231.
[41] D.S. Sigman, A. Mazumder, D.M. Perrin, Chem. Rev. 93 (1993) 2295–2316.
[42] Y. Wang, Z.Y. Yang, Q. Wang, Q.K. Cai, K.B. Yu, J. Organomet. Chem. 690 (2005) 4557–4563.
[43] J.Z. Wu, B.H. Ye, L. Wang, L.N. Ji, J.Y. Zhou, R.H. Li, Z.Y. Zhou, J. Chem. Soc., Dalton Tran. 8 (1997) 1395–1402.
[44] Y.C. Liu, Z.Y. Yang, J. Du, X.J. Yao, R.X. Lei, X.D. Zheng, J.N. Liu, H.S. Hu, H. Li, Chem. Pharm. Bull. 56 (2008) 443–451.
[45] Y.C. Liu, Z.Y. Yang, J. Du, X.J. Yao, R.X. Lei, X.D. Zheng, J.N. Liu, H.S. Hu, H. Li, Immunobiology 213 (2008) 651–661.

[46] L.A. Bagatolli, S.C. Kivatinitz, G.D. Fidelio, J. Pharm. Sci. 85 (1996) 1131–1132.
[47] M.M. Yang, P. Yang, L.W. Zhang, Chinese Sci. Bull. 9 (1994) 31–36.
[48] A. Ayar, B. Mercimek, Process Biochem. 41 (2006) 1553–1559.
[49] Z.L. Li, J.H. Chen, K.C. Zhang, M.L. Li, R.Q. Yu, Sci. China Ser. B: Chem. 11 (1991) 1193–1200.
[50] G. Scatchard, Ann. NY Acad. Sci. 51 (1949) 660–673.
[51] L.M. Berezhkovskiy, I.V. Astafieva, C. Cardoso, Anal. Biochem. 308 (2002) 239–246.
[52] J.B. Chaires, N. Dattagupta, D.M. Crothers, Biochemistry 21 (1982) 3933–3940.
[53] J.D. McGhee, P.H. von Hippel, J. Mol. Biol. 86 (1974) 469–489.
[54] M. Baldini, M. Belicchi-Ferrari, F. Bisceglie, G. Pelosi, S. Pinelli, P. Tarasconi, Inorg. Chem. 42 (2003) 2049–2055.
[55] J.-I. Ueda, N. Saito, Y. Shimazu, T. Ozawa, Arch. Biochem. Biophys. 333 (1996) 377–384.
[56] C.C. Winterbourn, Biochem. J. 198 (1981) 125–131.
[57] R. Xing, H. Yu, S. Liu, W. Zhang, Q. Zhang, Z. Li, P. Li, Bioorg. Med. Chem. 13 (2005) 1387–1942.
[58] F. Zsila, Z. Bikádi, M. Simonyi, Org. Biomol. Chem. 2 (2004) 2902–2910.
[59] A.G. Krishna, D.V. Kumar, B.M. Khan, S.K. Rawal, K.N. Ganesh, Biochim. Biophys. Acta 1381 (1998) 104–112.
[60] C.C. Winterbourn, Biochem. J. 182 (1979) 625–628.
[61] Z.Y. Guo, R.E. X, S. Liu, H.H. Yu, P.B. Wang, C.P. Li, P.C. Li, Bioorg. Med. Chem. Lett. 15 (2005) 4600–4603.
[62] G.M. Sheldrick, Acta Crystallogr. A 46 (1990) 467–473.